JOURNAL OF APPLIED ELECTROCHEMISTRY **26** (1996) 135–142

Theoretical and experimental studies of the effect of side reactions in copper deposition from dilute solutions on packed-bed electrodes

J. M. BISANG

Programa de Electroquímica Aplicada e Ingeniería Electroquímica (PRELINE), Facultad de Ingeniería Química, Universidad Nacional del Litoral, Santiago del Estero 2829, 3000 Santa Fe, Argentina

Received 5 December 1994; revised 6 June 1995

This paper analyses the effect of side reactions, such as the reduction of oxygen or Fe(III), on copper deposition from dilute acid sulfate solutions. Fundamental studies with a rotating disc electrode were performed to determine the potential regions where the reactions take place and also to calculate kinetic parameters under the conditions of the experiments. Applied studies carried out in a through-flow electrochemical reactor with a packed bed cathode formed by a stack of nets are reported. The experimental data are compared with theoretical results, according to the continuous model, to corroborate its reliability for the case of simultaneous electrochemical reactions. It was found that the agreement between the mathematical treatment and the experimental data is similar to the case of a single reaction in the electrode. Taking into account the side reactions, criteria for the selection of bed thickness parallel to the current flow are discussed.

List of symbols

a_e effective surface area per unit electrode volume (cm^{-1})
$a_{e,g}$ geometric surface area per unit electrode volume (cm^{-1})
C concentration ($mol\,cm^{-3}$, $mol\,dm^{-3}$ or p.p.m.)
C_i inlet concentration ($mol\,cm^{-3}$)
C_o outlet concentration ($mol\,cm^{-3}$)
D diffusion coefficient ($cm^2\,s^{-1}$)
d diameter of wire (cm)
E electrode potential (V)
E_0 reversible electrode potential (V)
E_0^0 reversible electrode potential under standard conditions (V)
$E_{1/2}$ half-wave potential (V)
F Faraday constant ($A\,s\,mol^{-1}$)
g weight of a net (g)
H distance between wires (cm)
I total current (A)
i current density ($A\,cm^{-2}$)
i_b macrokinetic current density ($A\,cm^{-2}$)
i_j current density of the jth reaction ($A\,cm^{-2}$)
$i_{L,j}$ limiting current density of the jth species ($A\,cm^{-2}$)
i_0 exchange current density ($A\,cm^{-2}$)
$i_{0,0}$ standard exchange current density
i_V total current per unit electrode volume ($A\,cm^{-3}$)
$i_{V,j}$ current of the jth reaction per unit electrode volume ($A\,cm^{-3}$)
j_D j factor for mass transfer $= (k/v)Sc^{2/3}$
k mass transfer coefficient ($cm\,s^{-1}$)
L bed thickness parallel to the current flow (cm)
N number of nets in the stack
R gas constant ($J\,K^{-1}\,mol^{-1}$)
Re Reynolds number $= vH/\nu\epsilon$
S cross-sectional area of the reactor (cm^2)
Sc Schmidt number $= \nu/D$
s_n normalized space velocity (s^{-1})
T Temperature (K)
v superficial liquid flow velocity ($cm\,s^{-1}$)
x axial coordinate in the direction of the current flow (cm)

Greek characters
β_j charge transfer coefficient of the jth electrode reaction
γ activity coefficient
δ density of the wires ($g\,cm^{-3}$)
ϵ screen volume void fraction
η overvoltage (V)
ν kinematic viscosity ($cm^2\,s^{-1}$)
$\nu_{e,j}$ charge number of the jth electrode reaction
ρ space time yield ($mol\,cm^{-3}\,s^{-1}$)
ρ_s^0 electrolyte resistivity ($\Omega\,cm$)
ρ_s effective electrolyte resistivity ($\Omega\,cm$)
ϕ potential (V)
ω angular velocity (s^{-1})

Subscripts
m main reaction
met metal phase
SCE saturated calomel electrode
s solution phase
sd side reaction

0021-891X

1. Introduction

Increasingly stringent legislation for effluents calls for reliable and cost-efficient processes for the purification of waste water. Kreysa [1] has recently reviewed the role of electrochemistry. Bennion and Newman [2] analysed, both theoretically and experimentally, copper deposition from dilute solutions using flow-through carbon electrodes. Additionally, in the last years new materials to construct three-dimensional electrodes have been investigated, such as carbon felts [3, 4], reticulated vitreous carbons [5–7] and metallic foams [8], which offer the advantages of a high value of both the specific surface area and the mass transfer coefficient and also a high permeability for the solution flow.

Moreover, during waste water treatment simultaneous electrochemical reactions take place at the electrode because of the complexity of the solutions involved. Therefore, the desired reaction occurs allied with side reactions which modify the current efficiency of the main reaction and also the current distribution in the electrode, thus altering its performance and affecting the reactor design. A few researchers have attempted to deal with electrochemical reactors with multiple reactions. Thus, Alkire and Gould [9] informed a very general theoretical analysis of multiple reaction sequences. Trainham and Newman [10] developed a model for flow-through porous electrodes operating above and below the limiting current of a metal deposition reaction and the results are compared with the experimental data for the deposition of copper from sulfate solutions with the simultaneous generation of dissolved hydrogen. Sabacky and Evans [11] presented a theoretical model for cylindrical fluidized bed electrodes of side-by-side configuration. In [12] experimental results for copper deposition in the presence of oxidizing agents were compared with theoretical predictions. Pletcher *et al.* [13] investigated the performance of reticulated vitreous carbon for the removal of copper ions from solutions of low ionic strength, saturated with air and/or containing chloride ion. Dew and Phillips [14] studied the effect of Fe(II) and Fe(III) on the efficiency of copper electrowinning with the Chemelec cell. Recently, Scott and Paton [15] analysed metal recovery by electrodeposition from mixed metal ion solutions in a batch recycle reactor. The mathematical treatment was compared with experimental results for electrodeposition of cadmium from solutions containing also ferric ions [16].

The purpose of the present work is to corroborate the reliability of the continuous model of three-dimensional electrodes when simultaneous reactions take place in it and to discuss some criteria for the selection of the bed thickness parallel to the current flow. It must be recognized that the side reactions considered here take place in the same potential range as the main reaction and, therefore, they can not be hindered by choice of the electrode potential.

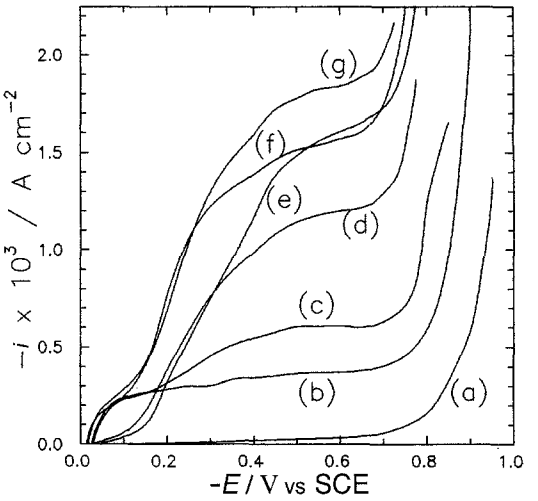

Fig. 1. Current density as a function of the electrode potential. Rotating disc electrode. Angular velocity 1000 r.p.m. $T = 30\,^{\circ}C$. (a) Hydrogen evolution from the supporting electrolyte (1 M Na_2SO_4 at pH 2). (b) Reduction of ferric ions from the supporting electrolyte with $[Fe^{3+}] = 50$ p.p.m. (c) Reduction of oxygen and ferric ions from aerated supporting electrolyte with $[Fe^{3+}] = 50$ p.p.m. (d) Copper deposition from the supporting electrolyte with $[Cu^{2+}] = 93$ p.p.m. (e) Copper deposition and reduction of oxygen. (f) Copper deposition and reduction of ferric ions. (g) Copper deposition and reduction of oxygen and ferric ions. Potential sweep rate 0.3 mV s^{-1}.

2. Fundamental studies with a rotating disc electrode

In these studies the working electrode was a copper rotating disc, 35 mm diameter embedded in a Teflon bell of 44 mm base diameter. The counter electrode was either a Pt-wire or a Cu-wire, in experiments involving copper deposition, in order to maintain a constant copper concentration. As reference, a saturated calomel electrode was used and all potentials are referred to this electrode. All experiments were performed at 30 °C under a slow potentiodynamic sweep and with a disc angular velocity of 1000 r.p.m. The supporting electrolyte was 1 M Na_2SO_4 with the addition of H_2SO_4 to achieve pH 2. The electrochemical reactions studied were copper deposition, as main reaction, and the reduction of oxygen and ferric ions as side reactions.

Figure 1 shows the experimental results. Curve (a) corresponds to hydrogen evolution from the supporting electrolyte. Prior to the measurements, dissolved oxygen was removed by bubbling nitrogen into the solution. It can be seen that hydrogen evolution becomes significant at potentials lower than −0.65 V. This value is the lowest cathode potential which may be tolerated in copper deposition to suppress hydrogen evolution. Curve (b) represents the reduction of ferric ions from oxygen free solution and curve (c) was obtained when this solution was saturated with air. In curves (b) and (c) the iron concentration was 50 p.p.m. Inspection of curve (b) reveals that a net reduction current for ferric ions is not observed until a potential of −0.025 V is achieved, which corresponds to the corrosion potential for copper in the presence of ferric ions. Curve (d) shows copper deposition from the supporting electrolyte with a copper concentration

of 93 p.p.m. Comparison between curves (b) and (d) shows that ferric ion reduction takes place preferentially to copper deposition and practically achieves limiting current condition before copper deposition occurs at appreciable rate. Comparison of curves (b), (c), and (d) shows that oxygen reduction on a copper electrode at pH 2, takes place simultaneously with copper deposition and with ferric ion reduction, in spite of the high value of the oxygen equilibrium potential. The additional experimental curves in Fig. 1 represent simultaneous reactions, for example, the cupric ion and oxygen reduction, curve (e), the cupric and ferric ion reduction, curve (f), and the oxygen, cupric and ferric ion reduction, curve (g), and are included in order to corroborate the studies with the single reactions. For example, it is observed that, within the accuracy normally expected for this type of measurement, curve (f) can also be obtained by addition of the copper deposition, curve (d), and ferric ion reduction, curve (b). This suggests that the reactions are independent of each other and, for engineering calculations, the global kinetics can be represented as the addition of the individual contribution of each reaction.

Curve (d) shows that copper deposition, considered in the following as the main reaction, shows combined diffusion and charge-transfer kinetic control and, consequently, can be modelled by the following expression:

$$i_m = \frac{\exp\left(\frac{\nu_{e,m}F}{RT}(E - E_0)\right) - 1}{\exp\left(\frac{\beta_m F}{RT}(E - E_0)\right)/i_0 - 1/i_{L,m}} \quad (1)$$

For the rotating disc electrode the limiting current density is given by

$$i_L = -0.62\nu_e F D^{2/3}\nu^{-1/6}\omega^{1/2}C \quad (2)$$

and according to [17]

$$i_0 = i_{0,0}C^{1-\beta_m/2} \quad (3)$$

The reversible electrode potential is given by the Nernst equation:

$$E_0 = E_0^0 + \frac{RT}{\nu_{e,m}F}\ln C\gamma \quad (4)$$

The experimental data for copper deposition shown in curve (d) of Fig. 1 were correlated by the least squares method in the form of Equation 1. Taking into account Equations 2, 3 and 4 the kinetic parameters gathered in Table 1 were obtained. The Table also shows the physicochemical properties of the solution. The kinetic parameters are in close agreement with previous values reported in the literature [17–19]. To calculate the reversible electrode potential for copper deposition the activity coefficient of the cupric ions was assumed equal to the mean ionic activity coefficient of the cupric sulfate, which was estimated using the method of Meissner [19].

Ferric ion reduction, considered in the following as a side reaction, is also under combined diffusion and charge-transfer control. However, because of the uncertainty in the calculation of its equilibrium potential the kinetics are expressed in terms of the half-wave potential, that is,

$$i_{sd} = \frac{i_{L,sd}}{1 + \exp\left(\frac{\beta_{sd}F}{RT}(E - E_{1/2})\right)} \quad (5)$$

To determine the kinetic parameters for ferric ion reduction the current densities, in the range of potentials between −0.05 and −0.15 V, were correlated by the least squares method, adjusting them to the logarithmic form of Equation 5. However, in the calculation it was preferred to use current densities obtained as the difference between the curves (f) and (d) in Fig. 1, instead of the similar polarization data given in curve (b), because the values of curve (b) are influenced by copper dissolution for potential values near the corrosion potential of copper. Likewise, the diffusion coefficient of the ferric ions was calculated from the limiting current density. The kinetic parameters for ferric ion reduction are also summarized in Table 1.

Table 1. Values of the physicochemical properties and the kinetic parameters of the reactions

Cu^{2+}/Cu	
	$\beta_m = 0.36$
	$i_0 = 1.13 \times 10^{-6}/C^{0.82}$ (p.p.m.)
	$D_{Cu^{2+}} = 5.58 \times 10^{-6}\ cm^2\ s^{-1}$
	$\nu_{e,m} = 2$
	$E_0^0 = 0.1$ V vs SCE
	$\gamma_{Cu^{2+}} = 0.0414$
Fe^{3+}/Fe^{2+}	
	$\beta_{sd} = 0.51$
	$D_{Fe^{3+}} = 3.35 \times 10^{-6}\ cm^2\ a^{-1}$
	$\nu_{e,sd} = 1$
	$E_{1/2} = -0.021$ V vs SCE

Solution: $[Cu^{2+}] = 93$ p.p.m, $[Fe^{3+}] = 50$ p.p.m. in 1 M Na_2SO_4 at pH 2.
$\nu = 1.11 \times 10^{-2}\ cm^2\ s^{-1}$.
$\rho^0 = 9.72\ \Omega$ cm.

3. Studies with packed-bed electrodes

3.1. *Summary of the mathematical model*

Taking into account the continuous model of three-dimensional electrodes, which considers that the electrode is formed by the overlapping of two continua: a solution phase and a conducting solid phase, and assuming that the effective resistivity of the solid phase is negligible, the mathematical description of the electrode is given by the following four equations: Current balance in the solution phase

$$\frac{di_s(x)}{dx} = a_e i(x) \quad (6)$$

where $i_s(x)$ is referred to the cross-sectional area in the direction of current flow and the starting position of the x-axis is arbitrarily set at the side of the packed-

bed electrode nearest to the counter electrode. Ohm's law for the solution phase

$$\frac{d\phi_s(x)}{dx} = -\rho_s i_s(x) \tag{7}$$

Definition of the local electrode potential

$$E(x) = \phi_{met}(x) - \phi_s(x) \tag{8}$$

The electrode potential is measured against any reference electrode, in this study the saturated calomel electrode.

Electrode kinetic expression

$$i(x) = i_m(x) + i_{sd}(x) \tag{9}$$

where the current density of the main reaction, $i_m(x)$, is given by Equation 1 and the current density of the side reaction by Equation 5. For the packed bed electrode the limiting current densities are given by

$$i_{L,j} = -\nu_{e,j} F k_p C_p \tag{10}$$

with $p = Cu^{2+}$ or Fe^{3+} for $j = m$ or sd.

The mass-transfer coefficient can be calculated from the correlation proposed by Cano and Böhm [21]

$$\epsilon j_D = 1.08\, Re^{-0.656}\,(H/d)^{0.333} \tag{11}$$

Combining Equations 6–8 results in the following differential equation

$$\frac{d^2E(x)}{dx^2} = \rho_s a_e i(x) \tag{12}$$

with the boundary conditions

$$x = 0 \qquad E = E(0) \tag{12a}$$

and

$$x = 0 \qquad \left.\frac{dE}{dx}\right|_0 = \rho_s i_b \tag{12b}$$

The effective electrolyte resistivity is given by the Bruggeman equation

$$\rho_s = \rho_s^0 \epsilon^{-3/2} \tag{13}$$

Taking into account the plug flow model, the concentration variation in the electrode is

$$\frac{dC_p(x)}{dx} = -\frac{i_j(x) a_e}{v \nu_{e,j} F} \tag{14}$$

with $p = Cu^{2+}$ or Fe^{3+} for $j = m$ or sd.

The macrokinetic current density, i_b, is obtained by integration of Equation 6

$$i_b = a_e \int_0^L i(x)\, dx \tag{15}$$

The geometric specific surface area and the screen volume void fraction are given by

$$a_{e,g} = \frac{4Ng}{d\delta SL} \tag{16}$$

and

$$\epsilon = 1 - \frac{Ng}{\delta SL} \tag{17}$$

To obtain the theoretical polarization curve for a packed-bed electrode, that is, i_b as a function of $E(0)$, Equations 12–17 were solved simultaneously with the kinetic expressions, Equations 1 and 5, and taking into account the Equations 3, 4, 10 and 11. The iterative solution of this system of equations was carried out numerically.

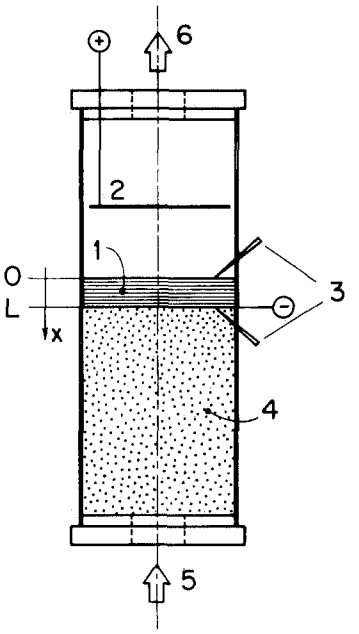

Fig. 2. Schematic representation of the reactor. (1) Three-dimensional electrode, (2) counter electrode, (3) reference electrodes, (4) glass beads, (5) electrolyte inlet, (6) electrolyte outlet.

3.2. *Experimental part and results*

All experiments were performed in a cylindrical electrochemical reactor, 44.35 mm internal diameter and 271 mm long, with parallel current and electrolyte flows, as shown schematically in Fig. 2. The working electrode was a stack of nets fabricated from discs of 50-mesh bronze screen, 0.15 mm wire diameter and 0.36 mm distance between wires, which were welded at several points in order to ensure isopotentiality of the metal phase. The geometric specific surface area was approximately 80 cm^{-1}. The upstream region of the stack, about 120 mm, was packed with glass beads, 4 mm diameter, to establish plug flow conditions in the working electrode and to decrease the entrance effects. A bundle of thin copper wires, 130 cm^2 surface area, was used as counter electrode, which was positioned downstream of the working electrode.

The experiments were performed potentiostatically, the working electrode potential was controlled with respect to a reference electrode at $x = 0$. The reactor was made part of a flow circuit system consisting of a reservoir, a pump, a flow meter and connections to maintain the temperature at the present value, 30 °C. The overall electrolytic volume was 5 dm^3 and the volumetric flow rate was 10 $dm^3\,min^{-1}$.

The electrolytic solution was 1 M Na_2SO_4 and H_2SO_4, to obtain pH 2, with a copper concentration of approximately 100 p.p.m. With this solution the

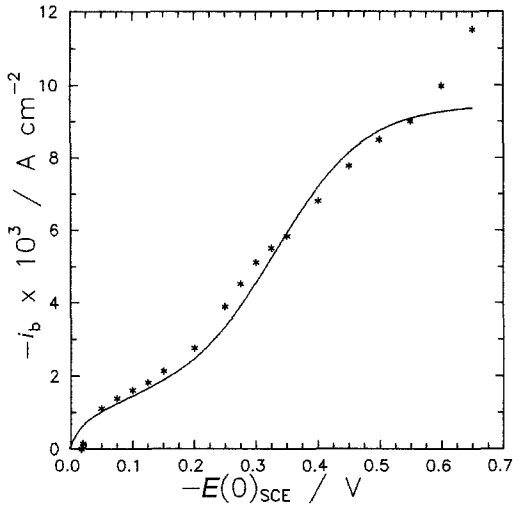

Fig. 3. Macrokinetic polarization curves for the simultaneous copper deposition and ferric ion reduction at an electrode with one net. Bed thickness = 0.03 cm. Full line: theoretical results. Electrolyte: 1 M Na_2SO_4, pH 2, $[Cu^{2+}] = 114$ p.p.m. and $[Fe^{3+}] = 48$ p.p.m. $T = 30\,^{\circ}C$.

stack of bronze nets was plated with copper. Immediately afterwards ferric sulfate was added to the solution to achieve an iron concentration of approximately 50 p.p.m. and the simultaneous reduction of cupric and ferric ions on the stack of copper plated nets was studied. The exact concentration of copper and iron was determined by atomic absorption spectroscopy and each experiment was carried out with a fresh solution. Nitrogen was bubbled into the reservoir to remove the dissolved oxygen. The time of operation was selected according to the electrolyte volume in order to obtain a small conversion and therefore to ensure approximately constant concentrations during the experiment.

Figures 3 and 4 show experimental data for stacks formed by different numbers of nets. In order to obtain agreement between the experimental results and the model it was necessary to use an 'effective

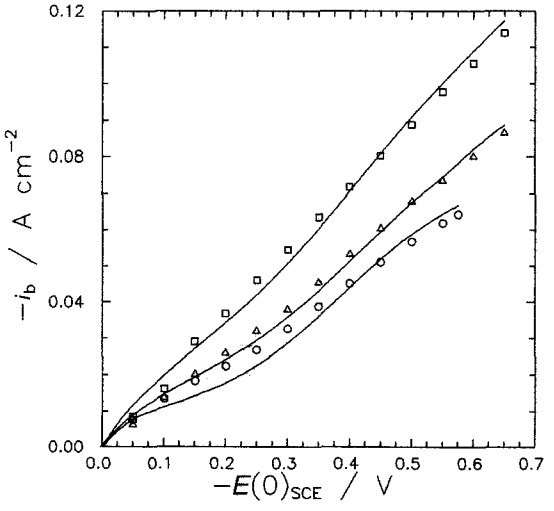

Fig. 4. Macrokinetic polarization curves for the simultaneous copper deposition and ferric ion reduction. (Number of nets, bed thickness/cm, $[Cu^{2+}]$/p.p.m., $[Fe^{3+}]$/p.p.m.): (○) 10, 0.31, 109, 50; (△) 25, 0.77, 125, 49; (□) 35, 1.1, 116, 49. Full lines: theoretical model. Supporting electrolyte: 1 M Na_2SO_4 at pH 2, $T = 30\,^{\circ}C$.

Table 2. Summary of the data correlation in Figs 3 and 4

Number of nets	$a_e/a_{e,g}$	*Mean relative deviation/%*
1	0.91	12.86
10	0.73	11.04
25	0.53	6.06
35	0.91	7.49

specific surface area' instead of the geometric specific surface area given by Equation 15. Therefore, the experimental results were correlated with the mathematical model by the least squares method using a_e as fitting parameter. The full lines in Figs 3 and 4 correspond to the theoretical results. It can be seen that the mathematical treatment is able to represent the behaviour of packed-bed electrodes when simultaneous reactions take place. Table 2 reports the ratio between the effective specific surface area from the correlation and the geometric value, Equation 16, together with the mean relative deviation for each case. It can be seen, with the only exception being the case of 25 nets, that the effective specific surface area is near to the geometric value. The small differences between them can be attributed to the difficulty in achieving high reproducibility in experiments on metal deposition. Table 2 also shows that the effective specific surface area is always smaller than the geometric value, which shows that in a packed-bed electrode the surface area is not fully used because the wires of the nets have a shielding effect, and also, from a microscopic point of view, each wire has a current distribution which varies with position on the surface. Therefore, the different regions of a wire do not offer the same contribution to the total current. This effect depends on the kinetic parameters of the test reaction and it is more significant when the contribution of charge-transfer is significant. Alkire and Gracon [22] obtained experimental results for a porous cathode fabricated from platinum screens. They adopted 0.81 as a multiplier of the specific surface area to obtain a good correlation when the test reaction was ferricyanide reduction. However, for copper deposition they found that experimental distributions were more nonuniform than those predicted on a theoretical basis. It must be recognized that analysis concerning the effectivity of the surface area in an electrode is only possible when the three-dimensional structure offers a well defined geometric area, such as is the case with a stack of nets. However, for other three-dimensional electrodes the above discussion is affected by uncertainty in the determination of a_e.

The full lines in Fig. 4 also show that when the bed thickness is high the macrokinetic current density increases monotonically with the applied potential, almost linearly with $E(0)$, and a limiting current density is not achieved. The three-dimensional structure shows a potential distribution in the direction of the current flow and when the test reaction has combined diffusion and charge-transfer

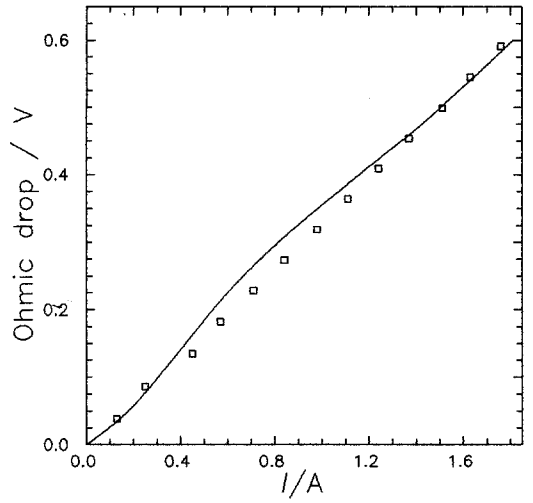

Fig. 5. Ohmic drop across the electrode as a function of the total current. 35 nets. Bed thickness = 1.1 cm. Full line: theoretical model. Electrolyte: 1 M Na_2SO_4 at pH 2, $[Cu^{2+}]=116$ p.p.m. and $[Fe^{3+}]=49$ p.p.m. $T=30\,^{\circ}C$.

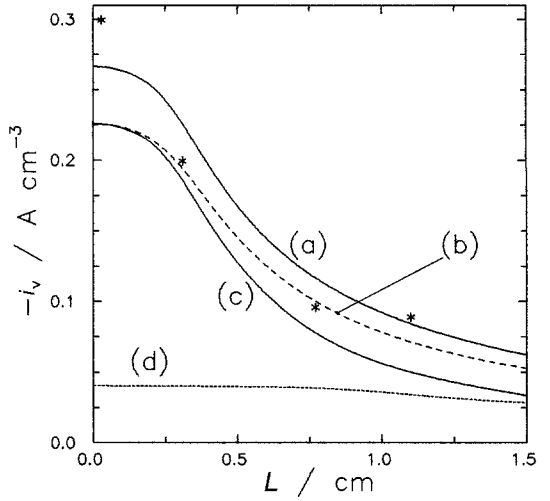

Fig. 6. Theoretical current per unit electrode volume as a function of the bed thickness. (a) Simultaneous copper deposition and ferric ion reduction. (b) Copper deposition as only reaction in the electrode. (c) Individual contribution of the copper deposition when occurs both reactions. (d) Individual contribution of the ferric ion reduction when occurs both reactions. $a_e = 62.15\,cm^{-1}$, $\epsilon = 0.7$, $E(0) = -0.55$ V, $[Cu^{2+}]=116$ p.p.m. and $[Fe^{3+}]=49$ p.p.m. $T=30\,^{\circ}C$. Other parameters according to Table 1.

kinetic control, such as in copper deposition, the electrode regions far from the counter electrode have a current density lower than the limiting value. This behaviour is emphasized when the mass transfer conditions are enhanced. Therefore, in mass transfer studies with packed-bed electrodes using copper deposition as test reaction, it is expected that, at low volumetric flow rates, the polarization curves show a limiting current density but when the volumetric flow rate is increased the limiting value is undefined.

To obtain additional confirmation of the mathematical model, in the experiment with the stack of 35 nets, two saturated calomel electrodes were used as reference electrodes, each being connected to Haber–Luggin capillaries. One of them was positioned in the side of the working electrode near the counter electrode, $x = 0$ in the mathematical model, and therefore measured the maximum potential of the stack of nets, while the second one was positioned at $x = L$ and measured the minimum potential. The difference between these potentials gave the ohmic drop in the stack of nets. The ohmic drop was measured for the stack of 35 nets, due to the fact that for thinner electrodes these measurements are more inaccurate. The results are shown in Fig. 5 as a function of the total current. The full line corresponds to the theoretical treatment. Close agreement between experimental and theoretical data is observed.

4. Engineering aspects of the model

In the design of electrochemical reactors with three-dimensional electrodes a fundamental aspect is the choice of bed thickness parallel to the current flow. Kreysa [23] proposed that the optimum bed depth is given by a maximum in the space time yield when a single reaction takes place under limiting current conditions. In previous work [24] this concept was extended for the case of cylindrical reactors. In the following this criterion will be discussed for the case where simultaneous electrochemical reactions takes place.

For the main reaction, the space time yield is related to the current per unit electrode volume through the equation [25]

$$\rho = \frac{i_{v,m}}{\nu_{e,m} F} \tag{18}$$

Another characteristic parameter of three-dimensional electrodes is the normalized space velocity, which is frequently used [26, 27] as a figure of merit for comparison of electrochemical reactors. The normalized space velocity for the main reaction is given by [25]

$$s_n = \frac{i_{v,m}}{(C_i - C_0)\nu_{e,m} F} \log\left(\frac{C_i}{C_0}\right) \tag{19}$$

where

$$i_{v,m} = \frac{a_e}{L}\int_0^L i_m(x)\,dx \tag{20}$$

obtained by the integration of Equation 6. In Equation 20, it was assumed that the reactor volume is equal to the electrode volume, which is a reasonable assumption for electrochemical reactors with three-dimensional electrodes. From Equation 18 it can be seen that the criterion of a maximum in the space time yield means a maximum in the current of the main reaction per unit reactor volume and also, according to Equation 19, a maximum in the normalized space velocity.

Figure 6 shows the current per unit electrode volume as a function of the bed thickness parallel to the current flow when copper deposition occurs as main reaction and, simultaneously, ferric ion reduction occurs as side reaction. For small values of L the i_v and $i_{v,m}$ curves show a small variation with L. In this region of L values the space time yield and the normalized space velocity are very close to their maximum values, which are only achieved for $L = 0$.

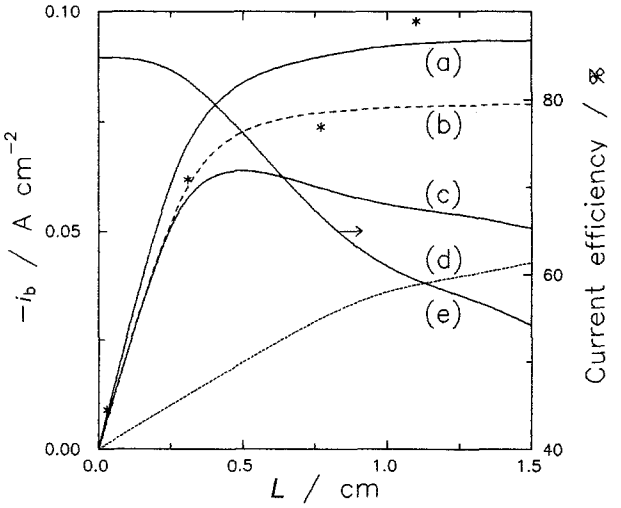

Fig. 7. Theoretical macrokinetic current density as a function of the bed thickness. (a) Simultaneous copper deposition and ferric ion reduction. (b) Copper deposition as only reaction in the electrode. (c) Individual contribution of the copper deposition when occurs both reactions. (d) Individual contribution of the ferric ion reduction when occurs both reactions. (e) Current efficiency for the copper deposition. $a_e = 62.15\,cm^{-1}$, $\epsilon = 0.7$, $E(0) = -0.55\,V$, $[Cu^{2+}] = 116$ p.p.m. and $[Fe^{3+}] = 49$ p.p.m. $T = 30\,°C$. Other parameters according to Table 1.

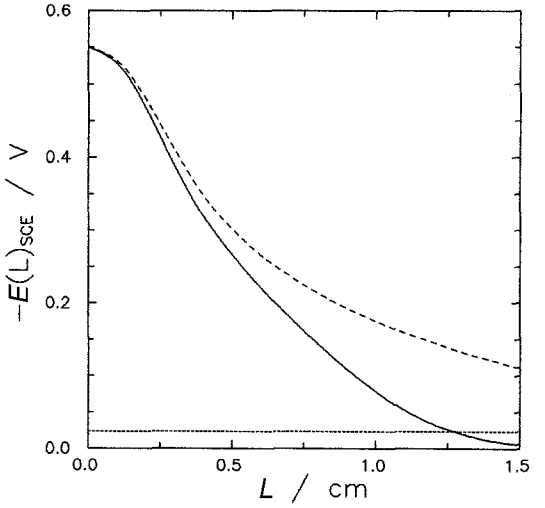

Fig. 8. Theoretical electrode potential at $x = L$ as a function of the bed thickness. Full line: simultaneous copper deposition and ferric ion reduction. Dashed line: copper deposition as only reaction in the electrode. Dotted line: reversible potential of the copper electrode. $a_e = 62.15\,cm^{-1}$, $\epsilon = 0.7$, $E(0) = -0.55\,V$, $[Cu^{2+}] = 116$ p.p.m. and $[Fe^{3+}] = 49$ p.p.m. $T = 30\,°C$. Other parameters according to Table 1.

But when L increases both curves decrease sharply. The curve for copper deposition as sole reaction, (dashed line), is also included in Figure 6 for comparison. For small thickness the side reaction does not influence the current of the main reaction per unit electrode volume, but its effect is significant as L increases because the side reaction alters the potential distribution in the electrode.

In Fig. 7 the macrokinetic current densities as a function of bed thickness are reported. The macrokinetic current density of the main reaction shows a maximum; this is a consequence of two opposite effects as L increases. In the first place an increase in L produces an increase in the surface area and, consequently, in $i_{b,m}$ but in the second place the increase in the surface area produces an increase in the current of the side reaction, dotted line in Fig. 7, which modifies the potential distribution in the electrode and causes a decrease in the current of the main reaction. Likewise, comparing curve (c) in Fig. 7 with the same curve of Fig. 6, it is seen that the maximum in the macrokinetic current density of the main reaction is achieved for a bed thickness higher than the L values for which, in Fig. 6, the current per unit electrode volume is high. Therefore, in the case of simultaneous reactions in a packed-bed electrode a maximum in the macrokinetic current density of the main reaction may be a criterion for the choice of bed thickness parallel to the current flow. From an economic point of view this criterion must be taken into account when the parts of the reactor related to the cross-sectional area in the direction of current flow, such as the counter electrode or the separator, represent predominant investment cost. The curve (e) in Fig. 7 gives the variation of the current efficiency for copper deposition as a function of the bed thickness.

The dashed line in Fig. 7 also shows the macrokinetic current density against L for the main reaction. The curve increases monotonically but its slope decreases with L. Therefore, for the case of a single reaction, analogously to i_v in Fig. 6, only considering i_b does not define an exact criterion for the choice of L and it is necessary to make an additional assumption, such as the Kreysa suggestion [23]. In Figs 6 and 7 experimental points taken from the polarization curves reported in Figs 3 and 4 are also included. It can be seen that the model follows the tendency of the experimental behaviour. The discrepancy between experimental and theoretical results may be attributed to the fact that the theoretical calculations were performed with mean values of concentrations and effective specific surface areas.

In Fig. 8 the electrode potential at $x = L$, as a function of L when $E(0) = -0.55\,V$, is shown. The full line corresponds to the case of simultaneous reactions and the dashed line to copper deposition as sole reaction. For the main reaction only, $E(L)$ tends asymptotically to the equilibrium potential as L increases. Therefore, in the case of a thick electrode the region farthest from the counter electrode is very inefficient, due to its low potential and it practically acts as current feeder for the active electrode region nearest to the counter electrode. However, the electrode behaviour is more complex when a side reaction also occurs and the equilibrium potential of the side reaction is higher than that of the main reaction. In this case, $E(L)$ decays with L and may reach values lower than E_0, because the current drained by the side reaction alters the potential distribution in the electrode. Figure 8 shows that, for $L \simeq 1.3\,cm$, $E(L)$ is equal to the equilibrium potential for copper deposition and for higher bed thicknesses an anodic zone occurs in the electrode. Therefore, in the case of packed-bed electrodes with simultaneous reactions

the potential at $x = L$ must be considered as a criterion to define a maximum value of the bed thickness which must not be exceeded in order to prevent the possibility of an inversion of the sign in the overpotential of the main reaction in the electrode region farthest from the counter electrode. It must be recognized that the inversion in the overpotential sign produces dissolution of the electrode material in the present case, but generates an inactive region when the three-dimensional structure is inert.

5. Conclusions

The following conclusions may be drawn:

(i) The mathematical treatment based on the continuous model of three-dimensional electrodes is appropriate for correlation of experimental results and is reliable in predicting the performance of packed-bed electrodes when the calculations are made with an 'effective specific surface area' instead of the geometric specific surface area. Laboratory experiments must be performed to determine the value of the effective specific surface area.

(ii) When simultaneous reactions take place the maximum in the macrokinetic current density of the main reaction must be considered in choosing the bed thickness parallel to the current flow.

(iii) When simultaneous reactions take place the bed thickness must not exceed a maximum value in order to avoid the possibility of inversion in the overpotential sign of the main reaction.

References

[1] G. Kreysa, *in* 'Ullmann's Encyclopedia of Industrial Chemistry', **A9** (1987) p. 227.
[2] D. N. Bennion and J. Newman, *J. Appl. Electrochem.* **2** (1972) 113.
[3] N. Vatistas, P. F. Marconi and M. Bartolozzi, *Electrochim. Acta* **36** (1991) 339.
[4] R. Carta, S. Palmas, A. M. Polcaro and G. Tola, *J. Appl. Electrochem.* **21** (1991) 793.
[5] M. Matlosz and J. Newman, *J. Electrochem. Soc.* **133** (1986) 1850.
[6] J. C. Card, G. Valentin and A. Storck, *ibid.* **137** (1990) 2736.
[7] D. Pletcher, I. Whyte, F. C. Walsh and J. P. Millington, *J. Appl. Electrochem.* **21** (1991) 659.
[8] A. Montillet, J. Comiti and J. Legrand, *ibid.* **24** (1994) 384.
[9] R. Alkire and R. Gould, *J. Electrochem. Soc.* **123** (1976) 1842.
[10] J. A. Trainham and J. Newman, *ibid.* **124** (1977) 1528.
[11] B. J. Sabacky and J. W. Evans, *ibid.* **126** (1979) 1176.
[12] *Idem, ibid.* **126** (1979) 1180.
[13] D. Pletcher, I. Whyte, F. C. Walsh and J. P. Millington, *J. Appl. Electrochem.* **21** (1991) 667.
[14] D. W. Dew and C. V. Phillips, *Hydrometallurgy* **14** (1985) 351.
[15] K. Scott and E. M. Paton, *Electrochim. Acta* **38** (1993) 2181.
[16] *Idem, ibid.* **38** (1993) 2191.
[17] R. Cabán and T. W. Chapman, *J. Electrochem. Soc.* **124** (1977) 1371.
[18] S. Morooka, K. Kusakabe, T. Watari and Y. Kato, *Int. Chem. Eng.* **21** (1981) 465.
[19] J. T. Hinatsu and F. R. Foulkes, *J. Electrochem. Soc.* **136** (1989) 125.
[20] C. L. Kusik and H. P. Meissner, *AIChE Symp. Ser.* **74** (1978) 14.
[21] J. Cano and U. Böhm, *Chem. Eng. Sci.* **32** (1977) 213.
[22] R. Alkire and B. Gracon, *J. Electrochem. Soc.* **122** (1975) 1594.
[23] G. Kreysa, *Electrochim. Acta* **23** (1978) 1351.
[24] G. Kreysa, K. Jüttner and J. M. Bisang, *J. Appl. Electrochem.* **23** (1993) 707.
[25] G. Kreysa, *ibid.* **15** (1985) 175.
[26] *Idem, Electrochim. Acta* . **11** (1981) 1693.
[27] F. C. Walsh, *ibid.* **38** (1993) 465.